Annals of the Academy of Romanian Scientists
Online Edition Series on Science and Technology of Information
ISSN 2066 - 2742 Volume **6**, Number **2**/**2013**

STUDY OF THE GRADIENT METHOD AIDED DARK CURRENT SPECTROSCOPY OF CCDS

Dan A. IORDACHE[1,2], Paul E. STERIAN[1,2], and Ionel TUNARU[3]

Abstract. *The Charge Coupled Devices (CCDs) have multiple applications as particle detectors, in astronomy, etc. Their characterization, by means of some accurate evaluations of their main physical parameters is always necessary. Besides the classical Deep-Level Transient Spectroscopy Method (DLTS), the Dark Current Spectroscopy (DCS) is the basic experimental method used in this aim. In the frame of the DCS method, the evaluation of the main parameters of CCDs is achieved starting from the temperature dependence of the dark current, usually by means of the classical gradient method (CGM), the final results being associated to the attraction centers (attractors) of the CGM application. Given being the studies of the basic features of this procedure are very rare, the main goal of this work is to achieve a systematic study of the basic features of attractors.*

Keywords: Charge Coupled Devices, Dark Current Spectroscopy, Temperature dependence of the dark current, Classical gradient method, Attractors

1. Introduction

The multiple uses of the Charge Coupled Devices (CCDs) [as particle detectors, in astronomy, etc.] were examined by the scientific monographs [1], [2]. The possibilities of identification of the contaminants and/or defects produced in the CCDs crystalline lattice were recently examined by us in the frame of the work [3].

Given being the complex character of CCDs, the evaluation of their physical parameters cannot be achieved by means of deterministic procedures, being necessary the use of some iterative procedures (by means of successive approximations), as that of the gradient method. In this case, the estimated values will correspond to the central part of some specific attractor's basins [4]. The identification of these central parts of the attractor's basins is achieved using the least squares principle, minimizing the sum:

$$S = \sum_{i=1}^{N} W_i (t_{i,calc.} - t_{i,\exp.})^2 \qquad (1)$$

of the weighted sum of the squares of deviations of the calculated values $t_{i,\ calc.}$ of the test parameters (of the dark current and different temperatures, particularly) relative to the experimental values $t_{i,\ exp.}$ (W_i is the weight associated to the test parameter i, where $i = 1, 2, \ldots N$).

[1] Prof., Physics Department, University of "Politehnica" Bucharest, Romania.
[2] Prof., Romanian Scientists Academy, Section of Information Science and Technology.
[3] Ph.D. student, Physics Department, University "Politehnica" of Bucharest, Romania.

Unfortunately, the practical use of the classical gradient method is sometimes hindered or misled by some specific numerical phenomena (instability, large oscillations, or pseudo-convergence, distortions, respectively) [5 - 8]. For the complex systems with several effective uniqueness parameters (as the CCDs), the intervening numerical phenomena are considerably more intricate than for the "mono-parameter" problems (e.g. the damped oscillator [9], the wave propagation in ideal media [5, 6], etc.).

For this reason, this work is intended to the examination of the basic features of the attraction basins for some (CCDs) complex systems with several effective uniqueness parameters.

In order to point out the basic features of the attractors, the following previous stages have to be studied: a) the rigorous quantum theory of the dark current in semiconductors, b) the choice of the corresponding dominant uniqueness parameters, c) the basic elements of the classical gradient method (CGM), d) choice of the zero-order approximations of the dominant uniqueness parameters and the study of the structure of the dark current sets at different temperatures; e) study of the convergence behavior of CGM, by means of some numerical experiments; f) the numerical phenomena associated to the CGM application on the EDCT, g) study of the strength levels of attractors, and only finally: h) the attractors basic features.

2. Rigorous Quantum Theory of the Dark Current in CCDs

The Charge Coupled Devices (CCDs) are complex systems, i.e. their rigorous (quantum) theoretical description requires the use of a huge number of (independent) uniqueness parameters (see e.g. [10], [11]). It is possible though to achieve some numerical descriptions of the complex systems in the limits of the existing experimental errors using a restricted (finite) number of uniqueness parameters, called "effective" parameters. In this aim, it is necessary to identify firstly the dominant uniqueness parameters, the effective ones being the dominant parameters that ensure a description of the studied complex system in the limits of the existing experimental errors.

The choice of the effective uniqueness parameters starts from the most accurate existing theoretical model of the studied complex system [12], [13]. As it was found, this "constitutive" theoretical model of the semiconductor materials involved by CCDs is the rather old, but still the most effective, SRH quantum model of Hall [14], Shockley and Read [15].

Inside the CCD region depleted of carriers, where n and $p << n_i$, the rigorous quantum SRH relations (1) and (5) of the work [16] lead to the following expression of the dark current:

$$j_{dark}(T) = j_{diff}(T) + T^{3/2} \cdot \exp\left(-\frac{E_g}{2kT}\right) \cdot c_n \frac{qV_{th}x_{dep}A_{pix}}{2} \sum_{k=1}^{n} \sigma_k N_{tk} \sec h\left[\frac{E_t - E_i}{kT} + pdg_{n,k}\right] \quad (2)$$

where n is the number of contaminant traps types, σ_k is the geometrical average ($\sqrt{\sigma_{nk}\sigma_{pk}}$) of the capture cross-sections of the free electrons and holes, respectively, and

$$pdg_{nk} \equiv d_{nk} = \arg\tanh\frac{\sigma_{nk} - \sigma_{pk}}{\sigma_{nk} + \sigma_{pk}} \left[= \frac{1}{2}\ln\left(\frac{\sigma_{nk}}{\sigma_{pk}}\right)\right] \quad (3)$$

is the polarization degree of the capture cross-sections corresponding to electrons (σ_{nk}) and holes (σ_{pk}), respectively, for the traps of type k.

Finally, the depletion dark current [the second term of relation (2)] can be described by the "global" expression:

$$j_{dep}(T) = q \cdot De^{-}_{0,dep.eff.} \cdot \sec h\left(\frac{E_t - E_i}{kT} + pdg_n\right)_{eff.} \cdot T^{3/2} \cdot \exp\left(-\frac{E_{g,eff.}}{2kT}\right) \quad (4)$$

where the effective depletion pre-exponential factor is a weighted sum [the weights being the hyperbolic secant factors: $\sec h\left(\frac{E_{tk} - E_i}{kT} + pdg_{n,k}\right)$] of the pre-exponential factors of each type of traps:

$$De^{-}_{0,trap\ k} = \frac{1}{2} x_{dep}A_{pix}c_n V_{th}\sigma_k N_{tk} \quad (5)$$

where N_{tk} is the number of traps of type k in the considered pixel.

Similarly, the effective value of the hyperbolic secant $\sec h\left(\frac{E_t - E_i}{kT} + pdg\right)_{eff.}$ is a weighted average of functions $\sec h\left(\frac{E_{tk} - E_i}{kT} + pdg_{n,k}\right)$ for each trap type, the corresponding weights being the pre-exponential factors $De^{-}_{0,trap\ k}$ for the trap type k.

For $|E_t - E_i| > 0.15$ *eV*, the depletion dark current will be less than 0.8% of its value for $E_t = E_i$, hence the depletion dark current will become negligible relative to the diffusion one, and its study by means of the DCS method will become very difficult or even practically impossible. For this reason - for the Widenhorn-Bodegom version [16], [10] of the DCS method - present interest only the **very** deep level traps, whose energies fulfill the condition: $|E_t - E_i| \leq 150$ meV.

Taking into account that the last sum of the expression (2) depends considerably on the trap type, the effective depletion current pre-exponential factor is in fact a weighted sum of the pre-exponential factors for each type of traps:

$$De^{-}_{0,trap\,k} = ½\, x_{dep} A_{pix} c_n V_{th} \sigma_k N_{tk}\ , \tag{6}$$

where σ_k and N_{tk} are the capture cross-section and the number of traps of type k in the considered pixel. Excepting the pixel area (A_{pix}), the values of the other 5 factors from the expression (2) of the depletion dark current pre-exponential factor: (i) the size x_{dep} of the depletion region, (ii) the pre-exponential factor $c_n = n_i \cdot T^{3/2} \cdot \exp(E_g/kT)$ of the intrinsic carrier concentration n_i, (iii) the thermal velocity V_{th} (due to its dependence $V_{th} = [8kT/(\pi \cdot m^*)]^{1/2}$ on the carrier effective mass), (iv) the capture cross-sections σ_k of the carriers of type k, and: (v) the concentration N_{tk} of the k-type of traps, are not accurately evaluated, their relative errors have frequently the magnitude order of 50%.

From relation (6) one finds that the contribution of **each** trap of type k to the depletion dark current pre-exponential factor is:

$$De^{-}_{0,trap\,k}/(x_{dep} A_{pix} N_{tk}) = ½\, c_n V_{th} \sigma_k \tag{5'}$$

hence the total depletion dark current pre-exponential factor corresponding to the studied pixel is:

$$De^{-}_{0,dep.pixel} = ½\, c_n\, \Sigma V_{th,k} \sigma_k N_{tk \in pixel} \tag{7}$$

The relation (7) allows the evaluation of the pre-exponential factor of the depletion dark current for each pixel, in terms of the parameters of the specific contaminants embedded in the considered pixel.

3. Choice of the Dominant Uniqueness Parameters

According to our studies, the most accurate expression of the dark current (as a sum of the diffusion and depletion dark current) in CCDs, using some effective parameters (averaged, in order to limit the number of the uniqueness parameters), is [3]:

$$De^{-}(T) = De^{-}_{diff}(T) + De^{-}_{dep}(T) =$$
$$= T^3 \exp\left(\ln De^{-}_{0,diff} - \frac{E_{g,eff.}}{kT}\right) + T^{3/2} \cdot \exp\left(\ln De^{-}_{0,dep} - \frac{E_{g,eff.}}{2kT}\right) \cdot \sec h\left[\frac{E_t - E_i}{kT} + d\right] \tag{8}$$

The accomplished study [17] pointed out the compatibility of the SRH quantum theoretical model with the existing experimental data for CCDs. A thorough examination of the expression (8) points out the following monotonic decreasing order of the 5 identified "effective" dominant uniqueness parameters in respect with their relative strength on the dark current values: a) the energy gap E_g (the strongest), then the natural logarithms of the: b) diffusion $\ln D^{-}_{0,diff.} \equiv \ln Diff$ and:

c) depletion $\ln D_{0,dep.}^{-} \equiv \ln Dep$ dark current (in this order), d) the difference $|E_t\text{-}E_i|$ of the energies corresponding to the embedded traps and to the intrinsic Fermi level, and: e) the polarization degree $d \equiv pdg$ (of weakest strength), respectively [3].

Unfortunately, the most important effective parameters for the identification of the defects and/or contaminants embedded in CCDs are the weakest strength ones: ln*Dep* (see also [17]), $|E_t - E_i|$ and $d \equiv pdg$ [3]. For this reason, the accuracy of these effective parameters evaluation will be carefully examined by this work.

4. Basic Elements of the Classical Gradient Method

As it is known, the classical gradient method aims to find the values of the effective uniqueness parameters (described by the column-vector $\bar{u}$), by means of the minimization of the sum S of weighted squares of the deviations of the calculated values $\bar{t}_{calc}(\bar{u}, \bar{s})$ relative to the corresponding experimental values $\bar{t}_{\exp}$:

$$S = \sum_{i=1}^{N} W_i (t_{calc.i} - t_{\exp.i})^2 = (\bar{t}_{calc.} - \bar{t}_{\exp.})^T \cdot \overline{\overline{W}} \cdot (\bar{t}_{calc.} - \bar{t}_{\exp.}) , \quad (9)$$

where $(\bar{t}_{calc.} - \bar{t}_{\exp.})^T$ is the transposed of the difference of the column-vectors $\bar{t}_{calc.}, \bar{t}_{\exp.}$, $\overline{\overline{W}}$ is the diagonal matrix of weights, and $\bar{s}$ is the vector of the state (or process) parameters.

The vector $\bar{C}^{(I)}$ of the corrections of the vector $\bar{u}$ of the uniqueness parameters in a certain successive approximation (iteration) I is obtained by means of the minimization condition of the sum S (exact if the functions $\bar{t}_{calc}(\bar{u}, \bar{p})$ would be linear):

$$\left[\frac{\partial (S^{(I)} + \delta S)}{\partial (\delta \bar{u})} \right]_{\delta \bar{u} = \bar{C}^{(I)}} = 0 \quad (10)$$

obtaining the expression [18]:

$$\bar{C}^{(I)} = -\left(\bar{\bar{J}}^{(I)T} \cdot \overline{\overline{W}} \cdot \bar{\bar{J}}^{(I)} \right)^{-1} \cdot \bar{\bar{J}}^{(I)T} \cdot \overline{\overline{W}} \cdot \bar{D}^{(I)} \quad (11)$$

where the Jacobean matrix $\bar{\bar{J}}^{(I)}$ is defined by its elements:

$$\left(\bar{\bar{J}}^{(I)} \right)_{ij} = \frac{\partial t_{calc.}^{(I)}}{\partial u_j} \quad (12)$$

and the deviation (column) vector is defined by the expression:

$$\overline{D}^{(I)} = \bar{t}_{calc.}^{(I)} - \bar{t}_{\exp} \tag{13}$$

where $\bar{t}_{calc.}^{(I)}$ is the column-vector of the calculated values of the test parameters in the iteration *I.*

An important feature of the gradient method efficiency is the so-called relative standard deviation, defined starting from the weighted sum of the deviations squares (9), by means of the expression:

$$\sigma(I) = \sqrt{\frac{S^{(I)}}{N}} = \sqrt{\frac{1}{N}\sum_{i=1}^{N}\left(t_{calc.i}^{(I)} - t_{\exp.i}\right)^2}\ , \tag{13}$$

where *N* is the number of the studied (independent) test parameters.

5. Choice of the zero-order approximations of the dominant uniqueness parameters. Study of the structure of the dark current sets at different temperatures.

It is very well known the extremely important role of the zero-order approximations to avoid the unpleasant numerical phenomena possibly intervening in the classical gradient method use.

The analysis of the main procedures used to choose the zero-order approximations corresponding to the numerical study of the temperature dependence of the dark current in CCDs [the so-called Dark Current Spectroscopy (DCS) method] points out the presence of 2 different strategies: a) that considering the whole ensemble of the existing experimental data [19], [16], b) the works preferring the choices of the zero-order approximations specific to the particular structure (for each pixel) of the experimental input data.

The first (general) procedure of the zero-order approximations choice starts from the overall analysis of the existing available results, defining these approximations by means of some average values for silicon: $\ln Diff^{(0)} \approx 34.9$ [16], p. 199, $\ln Dep^{(0)} \approx$ 19 [16], p. 200, E_g = 1.08 eV [19], fig. 2, p. 2557, the value E_g = 1.10 eV [19], p. 2556 being probably a rounded version of the previous one. We will mention also that all our numerical tests of the Sze [20] – Varshni [21] empirical expression:

$$E_g = E_{go} - \frac{\alpha \cdot T^2}{T + \beta}\ , \tag{14}$$

where E_{go} = 1.1557 [20] … 1.17 eV [21], $\alpha = 10^{-4}\ eV/K \times (7.021[21]...4.73[20])$, β = 1108 [20] … 636 K [21], led to considerable disagreements with the experimental data.

As it concerns the difference of energies of the traps and of the intrinsic Fermi level, respectively: $|E_t - E_i|$, the analysis of the numerical results presented by the synthesis works [22], [10], [3] shows that a reasonable value of the zero-order approximation is: $|E_t - E_i|^{(0)} \approx 0.1$ eV.

The second procedure of the zero-order approximations choice starts [10] from the least-squares fits of the temperature dependencies (specific to each pixel) of the dark current corresponding to the lowest (222… 242 K, field where the depletion dark current is prevailing) temperatures, and to the highest (272… 292 K, where the diffusion current prevails) ones, the indicated temperatures corresponding to the experimental studies [16], [10]. One finds [17] that the values of the zero-order approximations of the main uniqueness parameters can be evaluated by means of the relations:

$$E_g^{(0)} \cong -s_{diff} \cdot k \,,\quad \ln De_{0,diff}^{-} \cong c_{diff} - 3 \cdot \ln \tilde{T}_{diff} \,,\quad \ln De_{0,dep}^{-} \cong c_{dep} - \frac{3}{2} \ln \tilde{T}_{dep} - \ln 2 \,, \tag{15}$$

and:

$$|E_t - E_i|^{(0)} \cong \left(2 s_{diff} - s_{dep}\right) \cdot k \tag{16}$$

where $s_{diff.}$, s_{dep} and: $c_{diff.}$, c_{dep} are the slopes and the ordinates of the crossing points (intercepts), respectively, of the regression lines (least-squares fits) of the temperature dependencies of the dark current in the regions of prevalence of the diffusion, and of the depletion dark current, respectively:

$$\ln De_{diffusion prevailence}^{-} \cong c_{diff} - s_{diff} \cdot \frac{1}{T} \,,\quad \ln De_{depletion\ prevailence}^{-} \cong c_{dep} - s_{dep} \cdot \frac{1}{T} \,, \tag{17}$$

while $\tilde{T}_{diff}$, $\tilde{T}_{dep}$ are the average temperatures corresponding to the above indicated temperature ranges.

It results also [17] that the ratio of the slopes s_{dep}, s_{diff} corresponding to the depletion and diffusion prevalence, respectively, is:

$$\frac{s_{diff}}{s_{dep}} \cong \frac{2}{1 + 2|E_t - E_i| / E_g} \tag{18}$$

For the particular case of the strongest uniqueness parameter of the temperature dependence of the dark current of CCDs - the energy gap E_g, it is possible to find an efficient compromise of the 2 above presented methods of the zero-order approximation choice. In this aim, one observes that while: a) the Sze's limit for silicon: $E_{go} \approx 1.17$ eV is considerably larger than the usually accepted values (see e.g. [10]): $E_g = 1.08 \div 1.10$ eV, b) the modulus $E_{g,Lin}$ of the slope of the line joining the points corresponding to the extreme temperatures (222 and 291 K, for the

experimental data [16], [10]) of the plot $\ln De^{-}(T) = f\left(\frac{1}{kT}\right)$ is less than E_g (it is practically equal to E_g for the diffusion term of the dark current [first term in equation (8)], but it is considerably less than E_g (approximately equal to $E_g/2$) for the depletion term [the second one in (8)], the average value:

$$E_{g,Ave} = \frac{1}{2}\left(E_{go,Sze} + E_{g,Lin}\right) \tag{19}$$

can be used successfully as a zero-order approximation $E_g^{(0)} = E_{g,Ave}$ of the energy gap (together with the other "general" zero-order approximations, see above).

6. Study of the convergence behavior of the classical gradient method, by means of some numerical experiments

6.1. Evolution behavior similitude with the over-damped oscillators

The study (by means of some numerical experiments) of the convergence speed of the CGM [23] – [25], [18] (pp. 177-183), points out a certain similitude with the physics of the oscillators with frictions [4], with that of the over-damped oscillators [9] (p. 138), particularly. Table 1 and figures 1, 2 present some correspondences between the parameters and the evolutions of the: a) relative standard error in the frame of CGM aided DCS of CCDs (obtained by means of some numerical experiments) and: b) elongation of the over-damped mechanical oscillators (see also [18]). Figure 3 provides a simplified graphical explanation of the local climbing of the standard error hill (see fig. 1).

Table 1

Similitude between the evolutions in the non-periodic regime of the damped oscillators and those in the frame of the gradient method procedures, respectively

Over-damped mechanical oscillator	**Gradient method procedures**
x (space coordinate)	u (uniqueness parameter)
t (time)	I (iteration)
U (potential energy)	σ (relative standard error)
$\dot{x}$ (velocity)	$\partial u / \partial I$
Δs (change of minimized parameters)	$\Delta\tau$ (change of the minimized test parameters)
Δx (for 1 time step) $\propto \dot{x}$	$\Delta u = C \propto \frac{1}{J} \propto \frac{1}{\partial\tau / \partial u}$ (for an additional iteration)

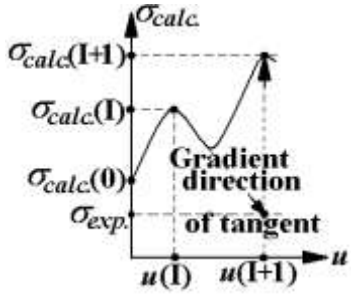

Fig. 1. Evolution types

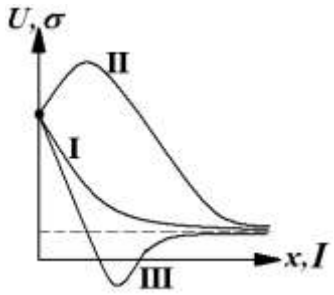

Fig. 2. Evolution vs. the potential and standard error hill profile.

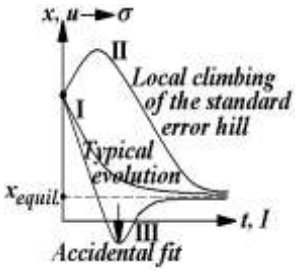

Fig. 3. Explanation of the local climbing of the standard error hill.

6.2. Numerical regularities in the successive approximations provided by the CGM for the evaluation of the main parameters of CCDs

This work studies the experimental data concerning the temperature dependence of the dark current in CCDs reported in the frame of the works [16] and [10]. Given being the approximately exponential rise of the dark current with temperature [see relation (8)], the values of the dark current at the lowest studied temperatures (222 and 232 K) are very small and the corresponding evaluation errors are rather high.

That is why our numerical results refer to the sets of the dark currents corresponding to the highest 6 temperatures studied by the works [16], [10] (between 242 and 291 K), and to the sets for all the 8 studied temperatures (from 222 to 291 K).

From the huge amount of obtained numerical data, we selected and we present in the frame of the Table 2 the found numerical regularities referring to the ratios of the successive relative standard errors $\sigma^{(I)}$ for the sets of studied temperatures, and of the deviations $D^{(I)}$ of the calculated dark current for some of the studied temperatures from the corresponding experimental values [10].

The obtained numerical data synthesized by Table 2 point out a new numerical phenomenon: the first 2 figures of the ratios of successive standard errors $\sigma(I)/\sigma(I+1)$ and deviations $D(I)/D(I+1)$ of the calculated dark current for some of the studied temperatures from the corresponding experimental values, respectively, are common for the first figures, for the first iterations.

Concerning the newly found numerical phenomenon, we can underline that its mechanism can probably be explained by means of the method of "transfer coefficients" (see e.g. [19], [20]), but its implementation will be considerably more difficult due to the multiple (independent) uniqueness parameters corresponding to this application.

Table 2

Calculated ratios of the successive relative standard errors $\sigma^{(I)}$ for some pixels and sets of studied temperatures, and of the deviations $D^{(I)}$ of the calculated dark current from the experimental value, respectively (see also [10])

Pixel	$\sigma(I)/\sigma(I+1)$ for 31;247		29; 88		
Iteration I	222…291 K	242…291 K	$\sigma(I)/\sigma(I+1)$ 242…291 K	$D(I)/D(I+1)$ for 232 K	$D(I)/D(I+1)$ for 291 K
1	1.309	1.300	2.723	2.731	2.720
2	1.287	1.286	2.728	2.741	2.723
3	1.287	1.286	2.744	2.740	2.731
4	1.287	1.286	2.789	2.732	2.751
5	1.288	1.287	2.920	2.749	2.810
6	1.289	1.287	3.330	2.817	2.979
7	1.290	1.288	4.886	3.081	3.515
8	1.291	1.289	4.941	4.492	5.753
9	1.292	1.290	1.0123	-5.733	422.984
10	1.294	1.292	1.0009252	-3.941	- 0.0658
11	1.295	1.293	1.00002024	0.378	1.08456
12	1.297	1.295	1.0000005399	1.098317	0.98708
13	1.299	1.297	1.0000000246	0.9835195	1.002218
14	1.300	1.300	0.99999999827	1.00285946	0.9996161
15	1.300	1.303	1.000000000232	0.99950476	1.00006653
16	1.300	1.305	0.9999999999629	1.00008583	0.99998847
17	1.291	1.308	1.000000000006524	0.99998512	1.000001998
18	1.277	1.311	0.9999999999988699	1.0000025779	0.9999996537
19	1.254	1.314	1.000000000000195	0.999999553	1.00000006001

By means of the above finding, it is possible to define the upper limit of the $I_{lin.}$ of this property (see Table 3). Similarly, it is possible to define the center $I_{steep.}$ of the steepest descent zone, as the value of the iteration I corresponding to the largest value of the ratio $\sigma(I)/\sigma(I+1)$. Finally, we can define the limits of the attractor's neighborhood region and of the attractor's central zone by means of the integers $I_{neighb.}$, $I_{centr.z.}$, as the nearest to the values $\ln\sigma(I) = -1.5 \rightarrow \sigma(I) \approx 0.223 \equiv 22.3\,\%$ and $\ln\sigma(I) = -4.0 \rightarrow \sigma(I) \approx 0.0183 \equiv 1.83\,\%$. In order to be possible to understand better the meaning of these notions, Table 3 below indicates the values of these 4 indices for the pixels and temperature ranges presented by Table 2.

Table 3

The values of the indices $I_{lin.}$, $I_{steep.}$, I_n and I_c for the pixels and sets of studied temperatures

Pixel	$\sigma(I)/\sigma(I+1)$ for 31;247		29; 88		
I_{index}	222…291 K	252…291 K	$\sigma(I)/\sigma(I+1)$ 252…291 K	$D(I)/D(I+1)$ for 232 K	$D(I)/D(I+1)$ for 291 K
$I_{lin.}$	13	13	4	4	5
$I_{steep.}$	15	23	7; 8	9	9
$I_{neighb.}$	21	21	8	2	- (never reached)
$I_{centr.z.}$	- (never reached)	30	≈ 10	4 … 5	- (never reached)

The above defined parameters allow to divide the attractor's space along the gradient procedure trajectory in 4 regions:

I. *The far linear (in* $\ln\sigma$*) ≡ exponential (in σ) regions of the attractor's basin*, between $\bar{u}^{(0)}$ and $\bar{u}^{(I_{\lim.})}$, where the last two vectors correspond to the ensembles of uniqueness parameters for the zero-order approximation and for the "limit" iteration with 2 common figures of the studied ratios,

II. *The steepest descent region,* between $\bar{u}^{(I_{\lim.})}$ and $\bar{u}^{(I_{neighb.})}$

III. *The attractor's neighborhood region,* between $\bar{u}^{(I_{neighb.})}$ and $\bar{u}^{(I_{centr.z.})}$

IV. *The attractor's central zone,* between $\bar{u}^{(I_{centr.z.})}$ and $\lim_{I\to\infty}\bar{u}^{(I)}$.

6.3. Descent of the relative standard error well (pit) in the frame of the successive approximations (iterations) of the classical gradient method used for the evaluation of the main parameters of CCDs

Given being the already reported results, we consider as the most suitable representation of the standard error well descent – the plot $\ln\sigma = f(I)$. To illustrate the above presented considerations, as well as to illustrate with some examples the typical evolutions of the classical gradient method procedure applied to the evaluation of the basic parameters of the temperature dependence of the dark current in CCDs, figures 4 and 5 indicate the plots $\ln\sigma = f(I)$ for the pixels 31, 247; 61, 140, and 121, 200, respectively.

Fig. 4 illustrates the 4 main regions of the attractor's space, along the direction of the gradient method procedure, for the versions of high accuracy (processing of the experimental results for the 6 higher temperatures: 242…291 K) and of lower accuracy (the above plot), of the classical evolution regime I of an over-damped oscillator (see fig. 1). Fig. 5 presents both the local climbing of the standard error hill (regime II) by means of the $\ln\sigma = f(I)$ plot corresponding to pixel 121, 200 (for the 6 higher temperatures 242…291 K), as well as the apparent "relaxation"

(regime III) after an accidental fit of the lowest level of the standard error. We have to mention also that: (i) the plot a) from figure 5 involves additionally multiple oscillations, as an effect of the several freedom degrees (described by E_g, ln*Diff*, ln*Dep* and $|E_t - E_i|$, (ii) the bottom of the standard error well can be determined more accurately by means of the method of *damped* gradient method (see e.g. [25]), which corrects the relation (11) by the introduction – in the zone of the studied pit bottom – of an attenuation factor λ (less than 1) suitably chosen:

$$\overline{C}^{(I)} = -\lambda \cdot \left(\overline{\overline{J}}^{(I)^T} \cdot \overline{\overline{W}} \cdot \overline{\overline{J}}^{(I)} \right)^{-1} \cdot \overline{\overline{J}}^{(I)^T} \cdot \overline{\overline{W}} \cdot \overline{D}^{(I)} . \qquad (11')$$

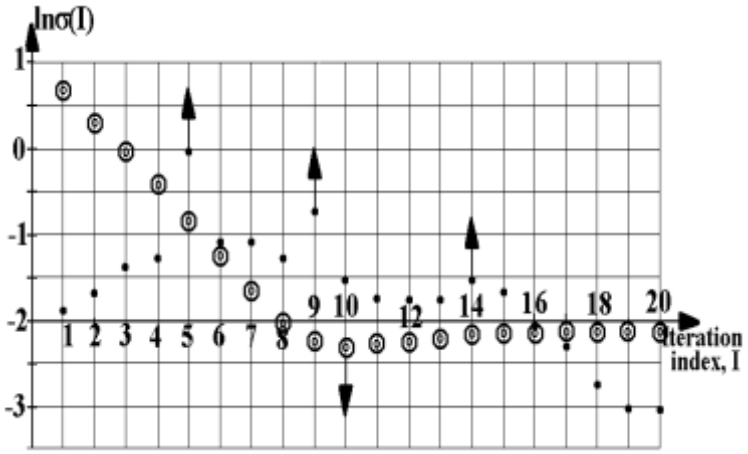

Fig. 4. Descent of the standard error well (pit) for the pixel 31, 247 and the ensembles of 8 temperatures 222…291 K (above) and 6 temperatures: 242…291 K (below).

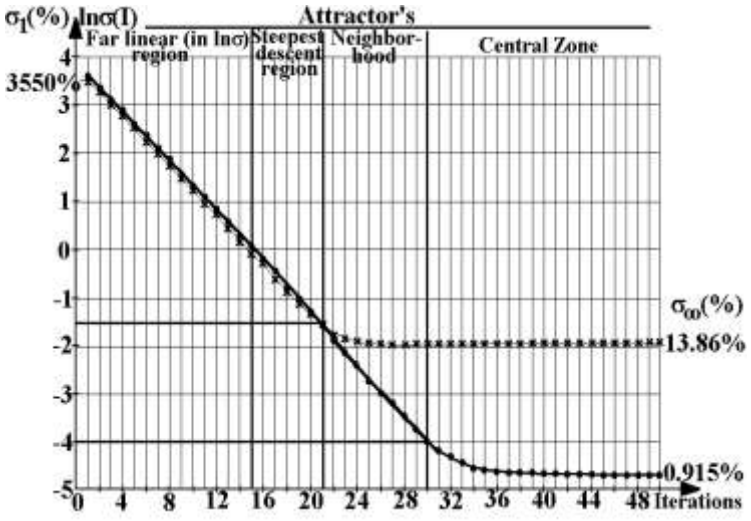

Fig. 5. a) Local climbings ↑ of the standard error hill (pixel 121, 200 for 242…291 K, plot marked by •),
b) Accidental identification ↓ of the standard error pit bottom
(pixel 61, 140, for all 8 temperatures, symbol ⊙), followed by "relaxation".

7. Study of the strength levels of attractors

7.1. Numerical Phenomena met in the frame of CGM aided DCS

Given being the following study will meet different types of typical numerical phenomena: a) Instability (symbol Inst.), b) Pseudo-Convergence (symbol Ps.), c) Oscillations (symbol Osc.), and – of course: d) the Convergence towards some specific (with physical meaning) attractors, denoted in terms of their strength: (i) VS (very strong), (ii) S (strong), (iii) MS (medium-strong), (iv) M (medium), (v) MW (medium-weak), (vi) W (weak), (vii) VW (very weak) and (viii) VVW (extremely weak), we synthesized in the illustrative figure 6 the typical appearance of these phenomena in the uniqueness parameters evaluation by the gradient method procedure (see also [17]).

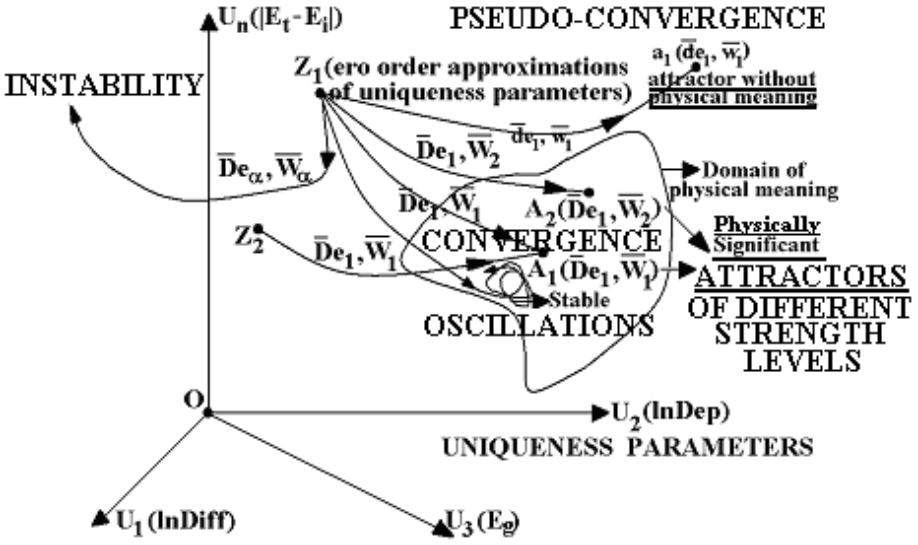

Fig. 6. Main types of numerical phenomena met in the evaluation of the uniqueness parameters by the gradient method.

7.2. Numerical experiments concerning the attractors strength levels

Taking into account that the usual single precision corresponds to 7 decimal places (for a 32-bit word machine [4], p. 23), it is possible to define the *strength levels of an attractor relative to a certain uniqueness parameter* by means of the number of common first decimals for several neighbor zero-order approximations: 7 common first decimals (VS), 6 (S), 5 (MS), 4 (M), 3 (MW), 2 (W), 1 (VW), 0 but a certain weak convergence (VVW). Of course, *the general attractor's strength level* will be its strength level relative to the weakest studied uniqueness parameters, i.e. relative to $|E_t - E_i|$ for the charge coupled devices.

Table 4

Final results concerning the values of the uniqueness parameters E_g, ln*Diff*, ln*Dep* and $|E_t - E_i|$, by means of the classical gradient method (for the experimental data see [16] and [10])

Coordinates of the pixel	E_g Zero-order Approximation M	$E_{g,eff.}$ (eV)	Ln*Diff*	ln*Dep*	$\|E_t - E_i\|$, meV	Numerical phenomenon & Attractor
61, 140	-10	**0.580869***	**9.402933***	**39.026176***	**381.94396***	**Pseudocon-vergence**
	-8	**0.564653***	**8.573753***	**40.444841***	**414.60294***	
	-6	1.072556	31.079047	17.52459	28.92168	**Very strong attractor**
	-4	1.072556	31.079047	17.52459	28.92168	
	-2	1.072556	31.079047	17.52459	28.92168	
	0	1.072556	31.079047	17.52459	28.92168	
	2	1.072556	31.079047	17.52459	28.92168	
	4	1.072556	31.079047	17.52459	28.92168	
	6; 8 & 10	**Instability** starting from iteration 4 (m = 6) and 2 (m = 8 and 10), resp.				
121, 200	-10	1.067221	30.865956	15.540974	13.31129	**Weak attractor; also, medium amplitude oscillations**
	-8	1.067238	30.866604	15.567840	12.93887	
	-6	1.067272	30.867992	15.659601	13.543185	
	-4	1.067263	30.867633	15.630247	13.350595	
	-2	1.067251	30.867136	15.596534	13.128485	
	0	1.067257	30.867372	15.611681	13.22839	
	2	1.067259	30.867458	15.617526	13.2669	
	4; 6; 8; 10	**Instability** from iteration 4 (m = 4) and 2 (m = 6; 8 and 10), respectively				
241, 320	-10	1.074871	31.172302	15.917362	11.094875	**Extremely weak attractor; also, large amplitude oscillations**
	-8	1.075900	31.212400	16.033195	9.955040	
	-6	1.075840	31.210004	16.349191	6.748465	
	-4	1.075873	31.211324	16.765059	8.779725	
	-2	1.075894	31.212169	15.976038	9.669870	
	0	1.075681	31.203713	15.338220	6.802035	
	2	1.075685	31.203874	15.336640	6.792465	
	4; 6; 8; 10	**Instability** from iteration 3 (m = 4) and 2 (m = 6; 8 and 10), resp.				
31, 247	-10	**0.587015***	**10.54143***	**44.932172***	**406.37874***	**Pseudocon-vergence**
	-8	**Instability** starting from iteration 9				
	-6	**0.574936***	**9.935104***	**45.115503***	**472.32972***	**Pseudocon-vergence**
	-4	**1.190187***	35.636207	19.734559	9.742655	**Extremely weak pseudo-attractor; also, large amplitude oscillations**
	-2	**1.190174***	35.635711	19.830541	10.175875	
	0	**1.190169***	35.635528	19.859227	10.302720	
	2	**1.190204***	35.636852	19.641657	9.317010	
	4	**1.190280***	35.639586	19.217493	7.276885	
	6	**1.190267***	35.639176	19.303182	7.692265	
	8; 10	**Instability** starting from iteration 2				

Taking into account that:

a) the effective energy gap $E_{g,eff.}$ is the strongest uniqueness parameter intervening in the description of the temperature dependence of CCDs dark current [see e.g. (8)],

b) the most efficient zero-order approximation of this parameter is given by the average value $E_{g,Ave}$, calculated by means of relation (19), starting from the Sze's general estimation $E_{g,Sze}$ and the so-called linear approximation $E_{g,Lin}$ (specific to each pixel), we will define the required successive neighbor zero-order approximations by means of the integer $m = \{-10, -8, -6, -4, -2, 0, 2, 4, 6, 8, 10\}$ and of the relation:

$$E_g^{(0)}(m) = E_{g,Ave} + \frac{m}{10}(E_{g,Sze} - E_{g,Ave}) . \qquad (20)$$

In this manner, the study of the attractor's strength levels becomes possible for all pixels, and we will select – by means of Tables 4 and 5 - only few, but most significant, particular examples.

Finally, a last question: could be possible to predict the convergence behavior of the gradient method procedure for the existing set of experimental data $De^- = f(T)$ corresponding to a certain pixel?

Obviously, the efficiency of the classical gradient method procedures depends on the accuracy of the chosen set of zero-order approximations.

That is why our analysis (see Table 5) will start from the zero-order approximations provided by the structures of the experimental data [see relations (15)-(18)].

We have to mention that the values of the effective uniqueness parameters of the 20 studied CCDs pixels were found [17] as located inside the intervals:

$E_g = 1.048...1.11 eV$, $\ln Diff = 30.19...32.36$, $\ln Dep = 14.59...19.41$ and $|E_t - E_i| = 6.8...45.4 eV$.

As it concerns the zero-order approximations, it is expected to be sometimes even outside these intervals, but not too much (for E_g and ln*Diff*, especially).

The symbols of the attractors' strength levels are indicated by bold characters in the last column of Table 5, while the atypical values of the zero-order approximations provided by the experimental data structure [relations (15)-(18)] are underlined.

Main parameters of the structure of the considered set of experimental data and the numerical phenomena intervening in the classical gradient procedure of evaluation of the main parameters of CCDs

Table 5

Studied pixel	$E_{g,eff.}^{(0)}$ (eV)	s_{diff} / s_{dep}	$\ln Diff^{(0)}$	$\ln Dep^{(0)}$	$\lvert E_t - E_i \rvert^{(0)}$ (meV)	Successive ($m\uparrow$) convergence behaviors
41, 120	1.0754	1.0948	31.2582	35.0979	443.8277	**Inst.**, Ps-converg.
61, 140	1.0951	1.8344	29.7980	16.2707	46.7512	Ps; **VS**; Inst.
81, 160	1.0573	1.6633	30.6121	19.5750	107.015	Ps; **MW**; Inst.
101, 180	1.0825	1.7172	31.6006	18.9916	89.1394	**W**
121, 200	1.0634	1.5713	30.8481	21.4230	145.0874	**W**
141, 220	1.0730	1.8727	31.2196	16.2769	36.4761	Ps; **W**; Inst.
161, 240	1.0833	1.6352	31.6390	20.5334	120.8284	Ps; Inst.; **VS**;Inst.
181, 260	1.0817	1.7283	31.5467	18.7122	85.0232	Ps; **W**; Inst.
201, 280	1.0667	1.7984	31.0414	18.1095	59.7857	Ps;Inst.;**MW**;Inst
221, 300	1.0801	1.9380	31.5415	16.1143	17.2792	Ps; **MS**; Inst.
241, 320	1.0647	1.5424	30.9015	22.1473	157.1197	**VVW**; Inst.
261, 340	1.0725	1.6102	31.2647	21.6275	129.8126	Ps; Inst.; **Ps**; Inst.
281, 360	1.0534	1.7251	30.5313	19.0919	83.9176	Ps; **VS**; Inst.
301, 380	1.0122	1.62016	28.9163	19.5766	118.6561	**Ps**; Inst.
321, 400	1.1261	1.6477	33.3843	20.8546	120.3996	Inst.; **MW**; Inst.
341, 420	1.0234	1.5826	29.3075	20.5133	134.943	Inst.; **Ps**; Inst.
29, 88	1.0950	1.6684	32.1206	20.8211	108.801	Ps; **MS**; Inst.
31, 247	0.9894	1.6873	27.9587	18.0671	91.6646	Ps; Inst.; **Ps**; Inst.
161, 289	1.1384	1.1654	33.7624	34.1341	407.632	**W**
188, 471	1.0888	1.7897	31.8896	17.6422	63.9686	**S**

The analysis of the results synthesized by Table 5 points out that:

a) the chosen definitions ensure a rather uniform distribution of the 20 CCD pixels indicated by work [10] over the attractors' strength levels: 3 very strong attractors (pixels 61, 140; 161, 240 and 281, 360), one strong attractor (pixel 188, 471), 2 medium-strong (29, 88 and 221, 300), 3 MW (81, 160; 201, 280 and 321, 400), 5 weak (101, 180; 121, 200; 141, 220; 181, 260 and 161, 289), one VVW

(241, 320), 4 pseudo-convergence cases (261, 340; 301, 380; 341, 420 and 31, 247) and a set of experimental data leading to instability (that of pixel 41, 120);

b) though there is a sure co-relation between the atypical values of certain zero-order approximations and the pseudo-convergence or instability of the gradient method iterative process, sometimes a set of atypical values of the zero-order approximations can equilibrate the computation system leading to some (of course, weak or very weak) physical attractors (see e.g. pixels 161, 289 or even 321, 400);

c) if the knowledge of the contaminants and/or defects embedded by the crystalline lattice if a certain pixel is important, but the structure of the first measurements (e.g. [10]) leads to pseudo-convergence of instability, it is necessary to repeat these measurements. The criterion of an accurate structure of the new set of experimental data is to find the inclusion of the zero-order approximations calculated by means of relations (15)-(18) in the already found intervals (see above and [17]).

8. Conclusions

This work studied the main features of the classical gradient procedure for some complex (with a huge number of uniqueness parameters) physical systems, i.e. for some particle detectors as the charge coupled devices (CCDs).

It was found that:

a) the effective (i.e. dominant parameters, used to reduce the number of the studied uniqueness parameters to a level allowing efficient computation procedures) uniqueness parameters have slightly, but different values than their corresponding physical parameters; e.g. while: (i) the physical energy gap E_g is temperature dependent, its associate effective parameter $E_{g,eff.}$ is temperature independent, (ii) the physical difference of energies of a certain trap (E_t) and of the intrinsic Fermi level (E_i): $|E_t - E_i|$ corresponds to a given contaminant or lattice defect, its effective parameter $|E_t - E_i|_{eff.}$ could be (if the studied pixel involves more than one type of traps) an average over the different types of involved traps,

b) the first iterations of the gradient method procedure present usually a monotonic (in arithmetic progression) decrease of the logarithm of the standard error $\ln\sigma$, i.e. a new numerical phenomenon, identified by this work,

c) using this newly found numerical phenomenon, it was possible to define the main domains of each attraction center (attractor): (i) *the linear* (in $\ln\sigma$, or exponential in the standard error σ) *field,* (ii) *the steepest descent region* of the standard error well (pit): $\ln\sigma = f(I)$, (iii) *the attractor's central zone* (for $\ln\sigma <$ -4), (iv) *the attractor's neighborhood* [for $\ln\sigma \in (-1.5; -4)$],

d) there were defined and determined for the sets of experimental data concerning the temperature dependence of the dark current corresponding to the 20 studied CCDs pixels [17] the attractors strength levels relative to: (i) each effective uniqueness parameter, (ii) a studied pixel. Given being that these strength levels are strongly related to the accuracy of the uniqueness parameters evaluation, their knowledge (and eventual improvement, by new measurements) seems to be essential for accurate assignments of the contaminants and/or defects embedded in the crystalline lattice of the pixels of certain particle detectors, as the charge coupled devices (CCDs) [3].

Acknowledgment

The authors thank very much to Professors Erik Bodegom and Ralf Widenhorn from the Physics Department of the Portland State University for the important awarded information and suggestions, as well as to the leadership of the Portland State University (Oregon, USA) for the Memorandum of Understanding 9908/March 6, 2006 – 2011 with University "Politehnica" of Bucharest, which allowed this cooperation.

REFERENCES

[1] J. R. Janesick, *Scientific charge-coupled devices*, SPIE Press, Bellingham, Wa, 2000, Appendices G1-G4, H1-H3.

[2] R. Widenhorn, *Charge Coupled Devices*, VDM, Saarbruecken, Germany, **2008**.

[3] D. Iordache, P. Sterian, I. Tunaru, *Charge Coupled Devices (CCDs) as Particle Detectors*, Hindawi, http://dx.doi.org/10.1155/2013/425746.

[4] R. H. Landau, M. J. Páez, *Computational Physics. Problem solving with Computers*, J. Wiley & Sons, New York - Chichester – Weinheim – Brisbane – Singapore – Toronto, **1997**.

[5] P. P. Delsanto, D. Iordache, C. Iordache, E. Ruffino, *Analysis of Stability and Convergence in FD Simulations of the 1-D Ultrasonic Wave Propagation*, in Mathl. Comp. Modelling, vol. **25**, no. 6, pp. 19-29, **1997**.

[6] D. Iordache, P. P. Delsanto, M. Scalerandi, *Pulse Distortions in the FD Simulations of Elastic Wave Propagation*, in Mathl. Comp. Modelling, vol. **25**, no. 6, pp. 31-43, **1997**.

[7] D. A. Iordache, *Contributions to the Study of Numerical Phenomena intervening in the Computer Simulations of some Physical Processes*, Credis Printing House, Bucharest, **2004**.

[8] D. A. Iordache, P. Sterian, F. Pop, A. R. Sterian, *Complex Computer Simulations, Numerical Artifacts, and Numerical Phenomena*, in Int. J. of Computers, Communications and Control, vol. **5**, no. 5, pp. 2010-2020, **2010**.

[9] E. Bodegom, D. Iordache, *Physics for Engineering students*, vol. 1, *Classical Physics*, Politehnica Press, Bucharest, **2007**.

[10] R. Widenhorn, E. Bodegom, D. Iordache, I. Tunaru, *Computational Approach to Dark Current Spectroscopy in CCDs as Complex Systems. I. Experimental Part and Choice of the Uniqueness Parameters*, in Sci. Bull. "Politehnica" Univ. Bucharest, Series A, vol. **72**, no. 4, pp. 197-208, **2010**.

[11] A. Sterian, P. Sterian, *Mathematical Models of Dissipative Systems*, in Quantum Engineering, vol. **2012**, Article ID: 367674, 12 pages (2012).

[12] R. Dobrescu, D. Iordache, eds., *Complexity Modeling* (in Romanian), Politehnica Press, Bucharest, **2007**.

[13] R. Dobrescu, D. Iordache, *Complexity and Information*, Romanian Academy Printing House, Bucharest, **2010**.

[14] R. N. Hall, *Electron-Hole Recombination in Germanium*, Phys. Rev. vol. **87**, p. 387, **1952**.

[15] W. Shockley, W. T. Read, *Statistics of the Recombination of Holes and Electrons*, in Phys. Rev., vol. **87**, p. 835, **1952**.

[16] R. Widenhorn, M. M. Blouke, A. Weber, A. Rest, E. Bodegom, *Temperature dependence of dark current in a CCD*, in Proc. SPIE Int. Soc. Opt. Eng., vol. **4669**, p. 193, **2002**.

[17] I. Tunaru, R. Widenhorn, D. Iordache, E. Bodegom, *Computational Approach to Dark Current Spectroscopy in CCDs as Complex Systems. II. Numerical Analysis of the Uniqueness*

Parameters Evaluation, in Sci. Bull. "Politehnica" Univ. Bucharest, Series A, vol. **73**, no. 1, pp. 149-162, **2011**.

[18] E. Bodegom, D. W. McClure, P. P. Delsanto, A. S. Gliozzi, D. A. Iordache, Fl. Pop, C. Roşu, R. Widenhorn, *Computational Physics Guide*, Politehnica Press, Bucharest, **2009**.

[19] R. D. McGrath, J. Doty, G. Lupino, G. Ricker, J. Vallerga, *Counting of deep-level traps using a Charge-Coupled Device*, in IEEE Trans. on Electron Devices, vol. **ED-34**, no. 12, pp. 2555-2557, **1987**.

[20] S. M. Sze, *Physics of Semiconductor Devices*, J. Wiley & Sons, **1981**.

[21] Y. P. Varshni, *Temperature dependence of the energy gap in semiconductors*, in Physica, vol. **34**, pp. 149-154, **1967**.

[22] W. C. McColgin, J. P. Lavine, C. V. Stancampiano, J. B. Russell, *Deep-level traps in CCD image sensors*, in Proc. Mater. Res. Symp., vol. **510**, pp. 475-480, **1998**.

[23] K. Levenberg, in *Quart. Appl. Math.* , p. 164, **1941**.

[24] D. W. Marquardt, *An algorithm for least-squares estimation of non-linear parameters*, in *J. of Soc. Industr. Appl. Math*., vol. **11**, pp. 431-441, **1963**.

[25] Z. Mei, J. W. Morris Jr., *Mössbauer Spectrum Curve Fitting with a Personal Computer*, in J. Nucl. Instrum. Methods in Phys. Res., vol. **6**, p. 371, **1990**.